

Heat transport in superionic materials via machine-learned molecular dynamics

Wenjiang Zhou^{1,2}, Benrui Tang³, Zheyong Fan³, Federico Grasselli^{4,5},

Stefano Baroni^{6,7*}, and Bai Song^{1,8*}

¹*School of Mechanics and Engineering Science, Peking University, Beijing 100871, China.*

²*School of Advanced Engineering, Great Bay University, Dongguan 523000, China.*

³*College of Physical Science and Technology, Bohai University, Jinzhou 121013, China.*

⁴*Department of Physics, Informatics and Mathematics, Università degli Studi di Modena e Reggio Emilia, Modena 41125, Italy.*

⁵*CNRNanoS3, Modena 41125, Italy.*

⁶*SISSA—Scuola Internazionale Superiore di Studi Avanzati, Trieste 34136, Italy.*

⁷*CNR-IOM—Istituto Officina Materiali, DEMOCRITOS SISSA Unit, Trieste 34136, Italy.*

⁸*National Key Laboratory of Advanced Micro and Nano Manufacture Technology, Peking University, Beijing 100871, China.*

*Corresponding author. Email: baroni@sissa.it (S. Baroni), songbai@pku.edu.cn (B. Song);

Abstract:

Precise modeling and understanding of heat transport in the superionic phase are of great interest. Although simulations combining Green-Kubo (GK) molecular dynamics with machine-learned potentials (MLPs) stand as a promising approach, substantial challenges remain due to the crucial impact of atomic diffusion. Here, we first show that the thermal conductivity (κ) of superionic materials calculated via conventional GK integral of the energy flux varies notably with the MLP model. Subsequently, we highlight that reliable, model-independent κ values can be obtained by applying Onsager's reciprocal relations to correctly capture the coupled heat and mass transport. Remarkably, an anomalously invariant κ is observed over a wide temperature range, distinct from the characteristic trends in traditional crystals and glasses. Finally, we illustrate that conventional κ decompositions into kinetic, potential, and cross terms suffer from ambiguities in the physical interpretation, despite their mathematical rigor.

Keywords: Superionic materials; Heat transport; Green-Kubo formalism; Onsager reciprocal relations; Machine-learned potentials.

The superionic phase is a unique intermediate state between crystalline solids and liquids [1-3], with a subset of ions exhibiting liquid-like mobility and diffusing almost freely through a rigid lattice formed by other ions that are localized and only vibrate around their equilibrium positions [3]. This intriguing phase has been observed in a variety of materials such as ice [4, 5], iron alloys [6], and helium-water compounds [7], and is attracting rapidly growing interest as a playground for fundamental research. In addition, superionic materials also hold great application potentials. Their high ionic conductivity at room temperature renders them promising candidates for next-generation energy storage technologies such as all-solid-state battery [8-10]. Further, their generally low thermal conductivity [11, 12], in conjunction with a relatively large electrical conductivity, makes them suitable for use in high-efficiency thermoelectric devices [12-14]. A notable example is the β -Cu₂Se-based superionic conductor, which has been reported to achieve a remarkable figure of merit of ~ 3.0 at 1050 K [14].

Key to the application of superionic materials is their thermal conductivity (κ) which, for example, is critical for battery thermal management [15] and largely determines the thermoelectric energy conversion efficiency [14, 16, 17]. However, the demand for very high pressures and temperatures presents a formidable obstacle to measuring some of the materials [6, 7], while those that could be measured yielded anomalously weak temperature dependences [18, 19]. Therefore, it is of fundamental importance to precisely model and understand thermal transport in the superionic phase. Unfortunately, the coexistence of solid- and liquid-like subsystems complicates first-principles calculations of κ [20-22]. Alternatively, Green-Kubo (GK) molecular dynamics (MD) [23, 24] empowered by machine-learned potentials (MLPs) [25-27] has emerged as a promising approach, which delivers quantum-mechanical accuracy at an affordable computational cost.

Within the conventional framework, κ is proportional to the GK integral of the energy flux [23, 24] defined as [28]:

$$\mathbf{J} = \mathbf{J}_{\text{kin}} + \mathbf{J}_{\text{pot}} = \frac{1}{V} (\sum_i \mathbf{v}_i \epsilon_i + \sum_i \mathbf{w}_i \cdot \mathbf{v}_i). \quad (1)$$

Here, \mathbf{J}_{kin} and \mathbf{J}_{pot} represent the kinetic and potential terms, respectively, which are also referred to as the convective and virial terms; and $\epsilon_i = m_i \mathbf{v}_i^2 / 2 + U_i$ denotes the atomic energy where \mathbf{v}_i , m_i , U_i , and \mathbf{w}_i are the velocity, mass, site potential, and per-atom virial of atom i , respectively. The kinetic term \mathbf{J}_{kin} is particularly important for heat conduction in superionic materials [29, 30]. However, a significant challenge arises: The site potential U_i is not uniquely defined in different MLP models even though the total energy remains consistent [31-33]. Furthermore, there is an additional non-uniqueness in the density-functional theory-based datasets used to train the MLPs [34], which occurs when the exchange-correlation functional is altered. These inherent ambiguities will inevitably limit the accuracy of the calculated κ values.

In this Letter, we explore thermal transport in two representative superionic materials, α -Li₃PS₄ and β -Cu_{1.98}Se, through the combination of Green-Kubo molecular dynamics with machine-learned potentials. We first show that the κ values computed via the conventional GK integral is strongly affected by the specific definition of the atomic site energy and thus by the choice of the MLP models. This issue is attributed fundamentally to the non-unique projection of the total energy onto the individual atoms, which has a major impact on heat transport in the presence of mass transport. Subsequently, by incorporating the Onsager reciprocal relations to properly account for the coupled transport, we obtain reliable and model-independent κ values. Remarkably, a nearly invariant κ is observed over a wide temperature range, which differs from traditional crystals and glasses but is reminiscent of previous experimental data for some other superionic materials [18, 19]. Finally, we discuss the decomposition of κ into kinetic, potential, and cross terms.

To begin with, we present a theoretical framework for calculating the thermal conductivity of superionic materials, which builds upon the conventional GK theory [23, 24] but incorporates the Onsager reciprocal relations [35, 36] to describe the coupled heat and mass transport. For a system with M distinct components (ions) in motion, there are M corresponding conserved fluxes J_i : One energy flux (denoted by subscript 0) and $M-1$ mass fluxes (since the total mass flux is constant). Any conserved flux can be expressed as a linear combination of the thermodynamic affinity F and the Onsager coefficient matrix Λ [35, 36]: $J_i = \sum_{j=0}^{M-1} \Lambda_{ij} F_j$. Each component Λ_{ij} can be obtained via the GK integral as [23, 24]:

$$\Lambda_{ij} = \frac{V}{k_B} \int_0^\infty \langle J_i(t) \cdot J_j(0) \rangle dt, \quad (2)$$

where $J_i(t) \cdot J_j(0)$ is the time correlation of the fluxes and $\langle \cdot \rangle$ denotes ensemble average. In a single-component system such as a typical solid, there is no mass flux and no contribution from the kinetic term \mathbf{J}_{kin} [37, 38]. Therefore, the thermal conductivity is simply given by the conventional GK formula as $\kappa = \Lambda_{00}/T^2$. This expression holds regardless of how the atomic energy (especially the site potential) is defined, which is known as the gauge invariance of thermal transport [39, 40].

In superionic materials with at least one moving component, the thermal conductivity is defined as the ratio of the energy flux to the temperature gradient under the condition that all other conserved fluxes are zero [29], and can be derived as $\kappa = 1/[T^2(\Lambda^{-1})_{00}]$. Specifically, in a two-component system, this expression simplifies to $\kappa = (\Lambda_{00} - \Lambda_{01}^2/\Lambda_{11})/T^2$. By introducing the notation $L_{ij} = \Lambda_{ij}/T^2$, the thermal conductivity can be concisely rewritten as:

$$\kappa = L_{00} - L_{01}^2/L_{11}. \quad (3)$$

Here, L_{00} is obtained through a direct GK integral of the energy flux which yields the thermal conductivity of a single-component system, while the subtracted term L_{01}^2/L_{11} accounts for the contribution of mass diffusion in a multi-component system. As will be shown later, this expression of κ satisfies both the gauge invariance principle [39] and the convective invariance principle [29], while L_{00} alone does not. Furthermore, based on the individual components of the energy flux in Eq. (1), the corresponding L_{00} can be decomposed into kinetic, potential, and kinetic-potential cross terms, which is expressed as: $L_{00} = \kappa_k + \kappa_p + 2\kappa_{kp}$. This decomposition of L_{00} has been widely employed to analyze thermal transport in superionic materials [11, 18, 33, 41-44] and will be revisited in this work.

Using the formalism described above, we first explore heat transport in α -Li₃PS₄, a promising solid-state electrolyte with a high ionic conductivity [45]. The training datasets are obtained from a previous study [46] which performed density-functional theory (DFT) calculations for various phases of Li₃PS₄ at the PBEsol level [47]. Specifically, we generate six pairs of datasets by randomly partitioning the original data into separate training and test datasets. Correspondingly, six MLP models are trained using the neuroevolution potential (NEP) framework [25, 48, 49], which are denoted as model A to F. All hyperparameters employed are the same as those used in Ref. [46]. The representative training process, along with the root-mean-square errors (RMSE) of energy, force, and virial stress are provided in Fig. S1 and Tables S1-S2 of the Supplemental Material [50].

With the trained MLP models at hand, we perform MD simulations using the GPUMD package [49, 51], with the details provided in the Supplemental Material [50]. In Fig. 1(a), we plot the calculated mean square displacement (MSD) of different species in α -Li₃PS₄ at selected temperatures from 350 K to 850 K. At relatively low

temperatures, α -Li₃PS₄ behaves like an ordinary solid, as indicated by the finite MSDs of all the atoms. However, as the temperature increases beyond 350 K, the MSD of the Li ions begins to diverge with the simulation time, while the P and S atoms remain finite, even at 650 K. This behavior clearly indicates transition into the superionic phase, which is further confirmed by the MD trajectories visualized in Fig. 1(a), with the Li ions traveling all over the system while the P and S atoms only vibrating around their equilibrium positions. In other words, at sufficiently high temperatures, α -Li₃PS₄ becomes a two-component superionic material, with Li⁺ diffusing within the solid framework formed by PS₄³⁻.

We further examine the projection of the total energy onto individual atoms, using models A and B as illustrative examples. As shown in Fig. 1(b), for the same α -Li₃PS₄ structure, while the difference in total energy is remarkably small (<0.3%) between the two MLP models, the distribution and magnitude of site potentials for the Li and S atoms differ significantly. This inherent non-uniqueness in decomposing the total energy strongly affects the simulation of thermal transport in superionic materials, which we will demonstrate later.

To calculate the thermal conductivity $\kappa = L_{00} - L_{01}^2/L_{11}$ of α -Li₃PS₄, we first conduct equilibrium MD simulations using the six MLP models to obtain the energy and mass fluxes. Then, the L_{00} , L_{01} , and L_{11} are computed with our in-house GK code, the details of which are provided in the Supplemental Material [50] together with some results for validation. In addition, we also calculate $\kappa = L_{00} - L_{01}^2/L_{11}$ by performing multivariate cepstral analysis (MCA) using the SporTran code [29, 52] which provides a benchmark. In Fig. 2(a), we plot representative κ values obtained at 650 K via different approaches for comparison. First, our GK code is validated by yielding essentially the same $L_{00} - L_{01}^2/L_{11}$ as that from MCA, using any one of the six MLP models. Further,

the $L_{00} - L_{01}^2/L_{11}$ values are highly consistent across different models, which are also in excellent agreement with previous reports [31, 46] and serve as a numerical manifestation of the convective invariance principle [29]. A mathematical proof is also provided in the Supplemental Material [50].

Compared to $\kappa = L_{00} - L_{01}^2/L_{11}$ which accounts for the coupled heat and mass flow, the widely used expression of $\kappa = L_{00}$ from conventional GK integral of the energy flux yields values that vary significantly across the six MLP models. With models A, E, and F, the calculated L_{00} values closely match $L_{00} - L_{01}^2/L_{11}$. However, with models B, C, and D, L_{00} is notably larger, reaching up to a factor of three. This model dependence renders the traditional use of $\kappa = L_{00}$ problematic for superionic materials and highlights the necessity of incorporating the Onsager reciprocal relations. Interestingly, the fact that half of the models yield fairly good predictions with $\kappa = L_{00}$ suggests that this problem can easily go unnoticed. To gain insight into the underlying mechanism, we further plot L_{01} and L_{11} in Fig. 2(b), observing that the former follows a trend similar to that of L_{00} while the latter remains consistent across different models. This indicates that the definition of atomic energy is key since it affects both L_{00} and L_{01} , while L_{11} only depends on the mass flux.

The temperature dependence of thermal conductivity provides valuable insights into the heat conduction mechanism [53-55]. In Fig. 3(a), we plot both the calculated L_{00} and $L_{00} - L_{01}^2/L_{11}$ as a function of temperature, using models A, C, and D as representative examples. At relatively low temperatures where the superionic diffusion is suppressed [see Fig. 1(a)], the contribution of \mathbf{J}_{kin} and the effect of heat-mass coupling are small [37, 38]. Consequently, the L_{00} values from the three models are similar. This observation may explain the wide and often successful adoption of L_{00} as the thermal conductivity of various solids. As the temperature rises, however, the three MLP models

exhibit distinct thermal transport behaviors: L_{00} increases rapidly for models C and D, while rising only slightly for model A. In contrast, $L_{00} - L_{01}^2/L_{11}$ yields very consistent values and a temperature-invariant trend across all three models. This behavior is highly unusual, since it differs both from the classical T^{-1} dependence of κ in typical crystals [56, 57] and the gradual increase of κ with T in amorphous materials [55, 58]. Interestingly, a recent study also reported a temperature-invariant thermal conductivity which was found in meteoritic silica between 80 K and 380 K [59]. In comparison, our results here cover a much wider temperature range from 350 K to 850 K, which reflects the distinctive thermal transport mechanism in superionic materials.

In Fig. 3(b), we further decompose L_{00} into κ_k , κ_p , and κ_{kp} as mentioned earlier. This approach has been widely employed to analyze why the thermal conductivity of superionic conductors deviate from the T^{-1} trend. At low temperatures, the potential term κ_p dominates and remains consistent across all three MLP models, while the kinetic term κ_k and the cross term κ_{kp} are nearly zero. However, as the temperature rises to the superionic range, a striking phenomenon is observed: κ_k , κ_p , and κ_{kp} all exhibit pronounced model-dependent variations. These results indicate that, although the energy flux-based decomposition is mathematically valid, it is not gauge invariant and lacks a clear physical interpretation.

In addition to α -Li₃PS₄, we consider β -Cu_{1.98}Se which exemplifies the superior thermoelectric potential of superionic materials [12-14]. At temperatures above 400 K [33], the Cu ions in this material exhibit liquid-like diffusion, while the Se ions vibrate around their equilibrium positions. We first construct four training datasets by employing the Vienna Ab initio simulation package (VASP) [60, 61], which results in four MLP models for subsequent MD simulations of thermal transport from 600 K to 1200 K [50]. As an example, Fig. 4(a) presents the computed L_{00} and $L_{00} - L_{01}^2/L_{11}$

values at 1000 K. As expected, the latter shows good consistency across all four MLP models and agrees well with the experimentally measured thermal conductivity minus the estimated electronic contribution [14]. Interestingly, in contrast to α -Li₃PS₄, L_{00} only shows a small model-induced variation of 8% and remains close to the experimental result.

To understand the distinct dependence of L_{00} on the MLP models in β -Cu_{1.98}Se, we examine the heat-mass coupling term L_{01}^2/L_{11} . As shown in Fig. 4(b), L_{01} also exhibits similar model dependence as L_{00} , whereas L_{11} shows a different trend and smaller variations. Compared β -Cu_{1.98}Se at 1000 K with α -Li₃PS₄ at 650 K, the calculated L_{01} are on the same order of magnitude, however, the values of L_{11} differ by a factor of 30. The much larger L_{11} in β -Cu_{1.98}Se leads to a very small correction (L_{01}^2/L_{11}) to L_{00} due to the heat-mass coupling, and therefore renders $\kappa = L_{00}$ a reasonable approximation. Despite the negligible model dependence of L_{00} , its decomposition into κ_k , κ_p , and κ_{kp} still appears rather arbitrary, as displayed in Fig. 4(c). This finding further reinforces the insight that it is unlikely to meaningfully resolve the individual contributions to thermal transport.

In contrast to our present results, previous simulations of β -Cu_{1.95}Se based on moment tensor potentials (MTP) reported L_{00} values that varied by a few fold across different models [33]. This could potentially be attributed to the particular energy flux formulation employed in the MTP, which has been demonstrated to be incorrect both in our previous work [38] and a similar study [62]. For verification, we deliberately employ an incorrect expression for the energy flux [50] and recalculate the thermal conductivity. As illustrated in Fig. 4(d), unlike the case with correct energy flux, this leads to substantial model dependence, with L_{00} differing by a factor of three between models A and D. Interestingly, even when using the incorrect energy flux, the values

computed via $L_{00} - L_{01}^2/L_{11}$ remain consistent and are relatively close to the correct result. This agreement, however, is likely a coincidence.

In summary, we have investigated heat transport in superionic materials via Green-Kubo molecular dynamics combined with machine-learned potentials. We first show that the conventional Green-Kubo approach are strongly dependent on the choice of MLPs and therefore problematic. Afterwards, we obtain reliable, model-independent κ values by applying Onsager’s reciprocal relations and incorporating a correction term that accounts for the heat-mass coupling. Intriguingly, across a wide temperature range of a few hundred kelvins, the κ of superionic materials appear to be almost invariant, which differs markedly from typical crystals and glasses. Finally, we show that the conventional decomposition of κ into kinetic, potential, and cross terms may not be physically meaningful. Our findings contribute to the precise modeling and understanding of thermal transport in the superionic phase, which may help advance applications such as all-solid-state batteries and efficient thermoelectric devices.

ACKNOWLEDGMENTS

We acknowledge Zezhu Zeng for helpful discussions on the Green-Kubo calculations. W.Z and B.S was supported by the Science Fund for Creative Research Groups from the National Natural Science Foundation of China (Grant No. 52521007), the Scientific Research Innovation Capability Support Project for Young Faculty (ZYGXQNJSKYCXNLZCXM-E1) from the Ministry of Education of China, the National Key R&D Program of China (Grant No. 2024YFA1207900), and the High-performance Computing Platform of Peking University. B.T. and Z.F. were supported by the National Science and Technology Advanced Materials Major Program of China (Nos. 2024ZD0606900 and 2025ZD0618902) and the Science Foundation from Education Department of Liaoning Province (No. LJ232510167001). B.S. acknowledges support from the New Cornerstone Science Foundation through the XPLOER PRIZE.

DATA AVAILABILITY

The training dataset of α -Li₃PS₄ is available at [63]. The training dataset, MLP models, as well as the main input and output of the MD simulations for β -Cu_{1.98}Se will be made freely available at [64]. The source code for Green-Kubo calculations also will be made freely available at [64]. Other data that support the findings of this work are available from the authors upon reasonable request.

References

- [1] J. B. Boyce and B. A. Huberman, Superionic conductors: Transitions, structures, dynamics, *Physics Reports* **51**, 189-265 (1979).
- [2] M. Parrinello, A. Rahman and P. Vashishta, Structural transitions in superionic conductors, *Physical Review Letters* **50**, 1073 (1982).
- [3] K. Funke, *Superionic solids and solid electrolytes recent trends* (Academic, San Diego, 1989).
- [4] P. Demontis, R. LeSar and M. L. Klein, New high-pressure phases of ice, *Physical Review Letters* **60** (22), 2284 (1988).
- [5] V. B. Prakapenka, N. Holtgrewe, S. S. Lobanov and A. F. Goncharov, Structure and properties of two superionic ice phases, *Nature Physics* **17** (11), 1233-1238 (2021).
- [6] Y. He, S. Sun, D. Y. Kim, B. G. Jang, H. Li and H. K. Mao, Superionic iron alloys and their seismic velocities in Earth's inner core, *Nature* **602** (7896), 258-262 (2022).
- [7] C. Liu, H. Gao, Y. Wang, R. J. Needs, C. J. Pickard, J. Sun, H.-T. Wang and D. Xing, Multiple superionic states in helium–water compounds, *Nature Physics* **15** (10), 1065-1070 (2019).
- [8] N. Kamaya, K. Homma, Y. Yamakawa, M. Hirayama, R. Kanno, M. Yonemura, T. Kamiyama, Y. Kato, S. Hama, K. Kawamoto, *et al.*, A lithium superionic conductor, *Nature Materials* **10** (9), 682-686 (2011).
- [9] Y. Li, S. Song, H. Kim, K. Nomoto, H. Kim, X. Sun, S. Hori, K. Suzuki, N. Matsui, M. Hirayama, *et al.*, A lithium superionic conductor for millimeter-thick battery electrode, *Science* **381**, 50–53 (2023).
- [10] G. Han, A. Vasylenko, L. M. Daniels, C. M. Collins, L. Corti, R. Chen, H. Niu, T. D. Manning, D. Antypov, M. S. Dyer, *et al.*, Superionic lithium transport via multiple coordination environments defined by two-anion packing, *Science* **383**, 739–745 (2024).
- [11] Q. Ren, M. K. Gupta, M. Jin, J. Ding, J. Wu, Z. Chen, S. Lin, O. Fabelo, J. A. Rodriguez-Velamazán, M. Kofu, *et al.*, Extreme phonon anharmonicity underpins

superionic diffusion and ultralow thermal conductivity in argyrodite Ag_8SnSe_6 , *Nature Materials* **22** (8), 999-1006 (2023).

[12] H. Liu, X. Shi, F. Xu, L. Zhang, W. Zhang, L. Chen, Q. Li, C. Uher, T. Day and G. J. Snyder, Copper ion liquid-like thermoelectrics, *Nature Materials* **11** (5), 422-425 (2012).

[13] Z. Zhou, Y. Huang, B. Wei, Y. Yang, D. Yu, Y. Zheng, D. He, W. Zhang, M. Zou, J.-L. Lan, *et al.*, Compositing effects for high thermoelectric performance of Cu_2Se -based materials, *Nature Communications* **14**, 2410 (2023).

[14] H. Hu, Y. Ju, J. Yu, Z. Wang, J. Pei, H. C. Thong, J. W. Li, B. Cai, F. Liu, Z. Han, *et al.*, Highly stabilized and efficient thermoelectric copper selenide, *Nature Materials* **23** (4), 527-534 (2024).

[15] Z. Rao, P. Lyu, M. Li, X. Liu and X. Feng, A thermal perspective on battery safety, *Nature Reviews Clean Technology* **1** (1), 511–524 (2025).

[16] W. Zhou, Y. Dai, T.-H. Liu and R. Yang, Effects of electron-phonon intervalley scattering and band non-parabolicity on electron transport properties of high-temperature phase SnSe : An ab initio study, *Materials Today Physics* **22**, 100592-100598 (2022).

[17] Y. Dai, W. Zhou, H.-J. Kim, Q. Song, X. Qian, T.-H. Liu and R. Yang, Simultaneous enhancement in electrical conductivity and Seebeck coefficient by single-to double-valley transition in a Dirac-like band, *npj Computational Materials* **8** (1), 234 (2022).

[18] M. K. Gupta, J. Ding, D. Bansal, D. L. Abernathy, G. Ehlers, N. C. Osti, W. G. Zeier and O. Delaire, Strongly anharmonic phonons and their role in superionic diffusion and ultralow thermal conductivity of Cu_7PSe_6 , *Advanced Energy Materials* **12** (23), 2200596 (2022).

[19] B. Li, H. Wang, Y. Kawakita, Q. Zhang, M. Feygenson, H. L. Yu, D. Wu, K. Ohara, T. Kikuchi, K. Shibata, *et al.*, Liquid-like thermal conduction in intercalated layered crystalline solids, *Nature Materials* **17** (3), 226 (2018).

- [20] A. Ward, D. Broido, D. Stewart and G. Deinzer, Ab initio theory of the lattice thermal conductivity in diamond, *Physical Review B* **80**, 125203 (2009).
- [21] L. Isaeva, G. Barbalinardo, D. Donadio and S. Baroni, Modeling heat transport in crystals and glasses from a unified lattice-dynamical approach, *Nature Communications* **10**, 3853 (2019).
- [22] M. Simoncelli, N. Marzari and F. Mauri, Unified theory of thermal transport in crystals and glasses, *Nature Physics* **15**, 809–813 (2019).
- [23] M. S. Green, Markoff random processes and the statistical mechanics of time-dependent phenomena. 2. Irreversible processes in fluids, *Journal of Chemical Physics* **22** (3), 398-413 (1954).
- [24] R. Kubo, Statistical-mechanical theory of irreversible processes. I. General theory and simple applications to magnetic and conduction problems, *Journal of the Physical Society of Japan* **12**, 570-586 (1957).
- [25] H. Dong, Y. Shi, P. Ying, K. Xu, T. Liang, Y. Wang, Z. Zeng, X. Wu, W. Zhou, S. Xiong, *et al.*, Molecular dynamics simulations of heat transport using machine-learned potentials: A mini-review and tutorial on GPUMD with neuroevolution potentials, *Journal of Applied Physics* **135** (16), 161101 (2024).
- [26] J. Behler and M. Parrinello, Generalized neural-network representation of high-dimensional potential-energy surfaces, *Physical Review Letters* **98** (14), (2007).
- [27] L. F. Zhang, J. Q. Han, H. Wang, R. Car and E. Weinan, Deep potential molecular dynamics: A scalable model with the accuracy of quantum mechanics, *Physical Review Letters* **120** (14), (2018).
- [28] Z. Fan, L. F. C. Pereira, H. Wang, J. Zheng, D. Donadio and A. Harju, Force and heat current formulas for many-body potentials in molecular dynamics simulations with applications to thermal conductivity calculations, *Physical Review B* **92** (9), 094301 (2015).

- [29] R. Bertossa, F. Grasselli, L. Ercole and S. Baroni, Theory and numerical simulation of heat transport in multicomponent systems, *Physical Review Letters* **122**, 255901 (2019).
- [30] W. Liu and Y. Zhou, Energy transport in superionic crystals, *Phys Rev Lett* **134** (14), 146301 (2025).
- [31] D. Tisi, F. Grasselli, L. Gigli and M. Ceriotti, Thermal conductivity of Li_3PS_4 solid electrolytes with ab initio accuracy, *Physical Review Materials* **8** (6), (2024).
- [32] P. Pegolo and F. Grasselli, Thermal transport of glasses via machine learning driven simulations, *Frontiers in Materials* **11**, 1369034 (2024).
- [33] Y. Zhu, E. Dong, H. Yang, L. Xi, J. Yang and W. Zhang, Atomic potential energy uncertainty in machine-learning interatomic potentials and thermal transport in solids with atomic diffusion, *Physical Review B* **108**, 014108 (2023).
- [34] S. Stackhouse, L. Stixrude and B. B. Karki, Thermal conductivity of periclase (MgO) from first principles, *Physical Review Letters* **104**, 208501 (2010).
- [35] L. Onsager, Reciprocal relations in irreversible processes. I, *Physical Review* **37**, 405-426 (1931).
- [36] L. Onsager, Reciprocal relations in irreversible processes. II, *Physical Review* **38**, 2265-2279 (1931).
- [37] W. Zhou and B. Song, Isotope effect on four-phonon interaction and lattice thermal transport: An atomistic study of lithium hydride, *Physical Review B* **110**, 205202 (2024).
- [38] W. Zhou, N. Liang, X. Wu, S. Xiong, Z. Fan and B. Song, Insight into the effect of force error on the thermal conductivity from machine-learned potentials, *Materials Today Physics* **50**, 101638 (2025).
- [39] A. Marcolongo, P. Umari and S. Baroni, Microscopic theory and quantum simulation of atomic heat transport, *Nature Physics* **12**, 80–84 (2016).
- [40] S. Baroni, The nuts and bolts of gauge invariance of heat transport. <https://doi.org/10.48550/arXiv.2509.17386>, 2025.

- [41] C. Wang and Y. Chen, Anisotropic phonon scattering and thermal transport property induced by the liquid-like behavior of AgCrSe₂, *Nano Lett* **23** (8), 3524-3531 (2023).
- [42] M. K. Gupta, J. Ding, H.-M. Lin, Z. Hood, N. C. Osti, D. L. Abernathy, A. A. Yakovenko, H. Wang and O. Delaire, Investigation of low-energy lattice dynamics and their role in superionic Na diffusion and ultralow thermal conductivity of Na₃PSe₄ as a solid-state electrolyte, *Chemistry of Materials* **36** (23), 11377-11392 (2024).
- [43] R. Cheng, W. Wang, W. Wang, X. Wang, C. Wang, S. T. Tai, N. Ouyang, Q. Liu and Y. Chen, Atomic hopping induced dynamic disorder phonon scattering and suppressed thermal transport in Cu₄TiSe₄, *Newton* **1** (4), 100090 (2025).
- [44] Y. Wang, R. Luo, J. Chen, X. Zhou, S. Wang, J. Wu, F. Kang, K. Yu and B. Sun, Proton collective quantum tunneling induces anomalous thermal conductivity of ice under pressure, *Physical Review Letters* **132**, 264101 (2024).
- [45] T. Kimura, T. Inaoka, R. Izawa, T. Nakano, C. Hotehama, A. Sakuda, M. Tatsumisago and A. Hayashi, Stabilizing high-temperature α -Li₃PS₄ by rapidly heating the glass, *Journal of the American Chemical Society* **145** (26), 14466-14474 (2023).
- [46] P. Pegolo, E. Drigo, F. Grasselli and S. Baroni, Transport coefficients from equilibrium molecular dynamics, *The Journal of Chemical Physics* **162**, 064111 (2025).
- [47] J. P. Perdew, A. Ruzsinszky, G. I. Csonka, O. A. Vydrov, G. E. Scuseria, L. A. Constantin, X. L. Zhou and K. Burke, Restoring the density-gradient expansion for exchange in solids and surfaces, *Physical Review Letters* **100**, 136406 (2008).
- [48] Z. Fan, Z. Zeng, C. Zhang, Y. Wang, K. Song, H. Dong, Y. Chen and T. Nissila, Neuroevolution machine learning potentials: Combining high accuracy and low cost in atomistic simulations and application to heat transport, *Physical Review B* **104** (10), 104309 (2021).
- [49] K. Xu, H. Bu, S. Pan, E. Lindgren, Y. Wu, Y. Wang, J. Liu, K. Song, B. Xu, Y. Li, *et al.*, GPUMD 4.0: A high-performance molecular dynamics package for versatile materials simulations with machine-learned potentials, *MGE Advances* **3**, e70028 (2025).

- [50] See Supplemental Material for the computational methods, machine-learned potential models, simulation models, validation of the code, size effect test, EMD and HNEMD simulations, Onsager coefficients, thermal conductivity decomposition, effect of energy flux, which includes Refs. [46, 48, 51, 60, 61].
- [51] Z. Fan, H. Dong, A. Harju and T. Ala-Nissila, Homogeneous nonequilibrium molecular dynamics method for heat transport and spectral decomposition with many-body potentials, *Physical Review B* **99** (6), 064308 (2019).
- [52] L. Ercole, R. Bertossa, S. Bisacchi and S. Baroni, SporTran: A code to estimate transport coefficients from the cepstral analysis of (multivariate) current time series, *Computer Physics Communications* **280**, 108470 (2022).
- [53] Z. Zeng, Z. Fan, M. Simoncelli, C. Chen, T. Liang, Y. Chen, G. Thornton and B. Cheng, Lattice distortion leads to glassy thermal transport in crystalline $\text{Cs}_3\text{Bi}_2\text{I}_6\text{Cl}_3$, *Proceedings of the National Academy of Sciences of the United States of America* **122** (41), e2415664122 (2025).
- [54] W. Zhou, Y. Dai, J. Zhang, B. Song, T.-H. Liu and R. Yang, Effect of four-phonon interaction on phonon thermal conductivity and mean-free-path spectrum of high-temperature phase SnSe, *Applied Physics Letters* **121** (11), 112202 (2022).
- [55] Z. Zeng, X. Liang, Z. Fan, Y. Chen, M. Simoncelli and B. Cheng, Thermal transport of amorphous hafnia across the glass transition, *ACS Materials Letters* **7** (8), 2695-2701 (2025).
- [56] X. Wu, W. Zhou, H. Dong, P. Ying, Y. Wang, B. Song, Z. Fan and S. Xiong, Correcting force error-induced underestimation of lattice thermal conductivity in machine learning molecular dynamics, *The Journal of Chemical Physics* **161**, 014103 (2024).
- [57] W. Yan, Y. Xue, W. Zhou, Y. Wang, H. Guo, H. Yang, H. Yang, Z. Jiang, L. Ding, W. Chen, *et al.*, Au ion irradiation induces ultralow thermal conductivity in GaN, *Applied Physics Letters* **125**, 032202 (2024).

- [58] Y. X. Wang, N. J. Liang, X. X. Zhang, W. J. Yan, H. Y. He, A. Fiorentino, X. W. Tao, A. Li, F. W. Yang, B. X. Li, *et al.*, Thermal transport in a 2D amorphous material, *Physical Review X* **15** (3), 031077 (2025).
- [59] M. Simoncelli, D. Fournier, M. Marangolo, E. Balan, K. Béneut, B. Baptiste, B. Doisneau, N. Marzari and F. Mauri, Temperature-invariant crystal–glass heat conduction: From meteorites to refractories, *Proceedings of the National Academy of Sciences of the United States of America* **122** (28), e2422763122 (2025).
- [60] P. E. Blochl, Projector augmented-wave method, *Physical Review B* **50** (24), 17953-17979 (1994).
- [61] J. P. Perdew, K. Burke and M. Ernzerhof, Generalized gradient approximation made simple, *Physical Review Letters* **77** (18), 3865-3868 (1996).
- [62] S. Tai, C. Wang, R. Cheng and Y. Chen, Revisiting many-body interaction heat current and thermal conductivity calculations using the moment tensor potential/LAMMPS interface, *Journal of Chemical Theory and Computation* **21**, 3649-3657 (2025).
- [63] <https://archive.materialscloud.org/records/4m62e-np961>.
- [64] <https://github.com/WenjiangZhou/Data-for-MyPub2>.

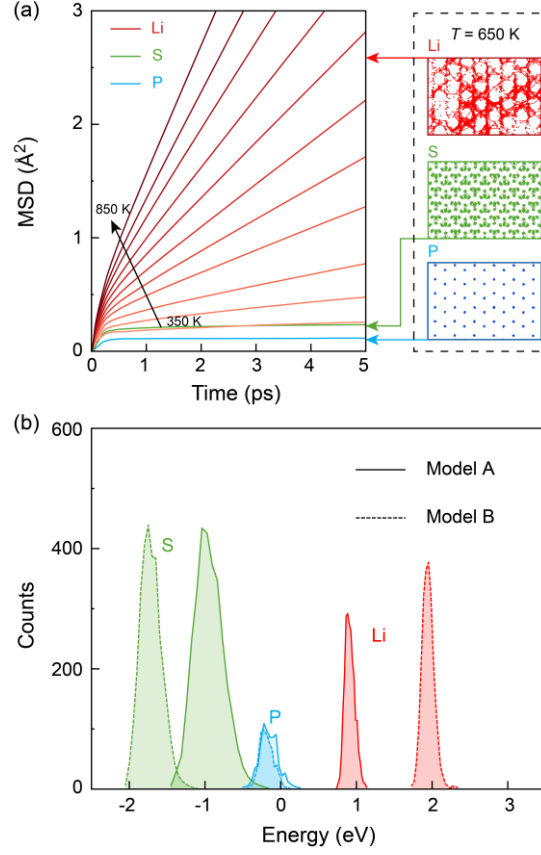


FIG. 1. Mean square displacement (MSD) and non-uniqueness of atomic projection of total energy in α -Li₃PS₄. (a) Calculated MSD of Li, P, and S atoms in α -Li₃PS₄ as a function of time and temperature. Results from 350 K to 850 K are shown for Li (red) in steps of 50 K; while for S (green) and P (blue), only the 650 K data are plotted for clarity. Right panel visualizes MD trajectories of the Li, S, and P atoms at 650 K from 1000 MD frames. Dots mark the atoms while lines trace their movement. For Li, the trajectories of only four atoms near the corner and one near the center are displayed. (b) Distribution of atomic energies in α -Li₃PS₄ for the same supercell structure. Results computed from two machine-learned models (A and B) are shown as an example.

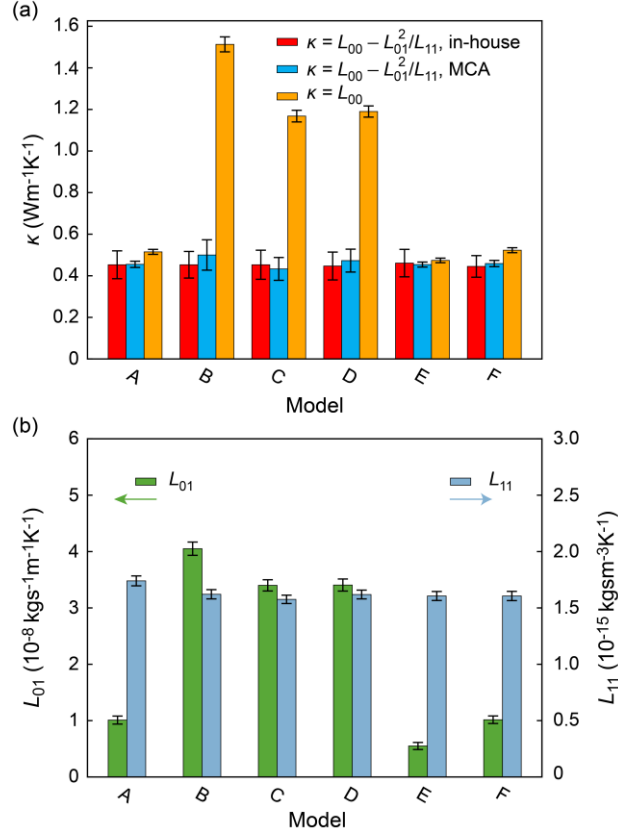


FIG. 2. Thermal conductivity and Onsager coefficients of α -Li₃PS₄ at 650 K. (a) Thermal conductivity values obtained from the conventional Green-Kubo integral based on L_{00} (orange) and also the formula $L_{00} - L_{01}^2/L_{11}$ which satisfies the invariance principle (red and blue). Here, the results from multivariate cepstral analysis (MCA, blue) are shown for comparison and validation [29]. Six different machine-learned models are considered, which are denoted as models A to F. (b) L_{01} (green, left axis) and L_{11} (blue, right axis) from different models.

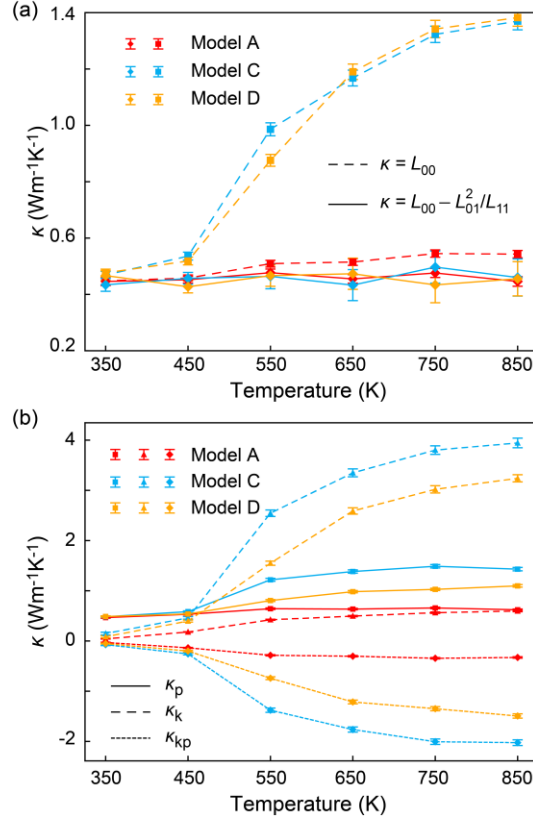


FIG. 3. Thermal conductivity of α -Li₃PS₄ and its decomposition based on energy flux as a function of temperature. (a) Thermal conductivity calculated from the Green-Kubo integral based on L_{00} (dashed lines) and also $L_{00} - L_{01}^2/L_{11}$ (solid lines) via the machine-learned models A (red), C (blue), and D (yellow). (b) Energy flux-based decomposition of the thermal conductivity (L_{00}) into κ_p , κ_k , and κ_{kp} , which represent contributions of the potential (solid), kinetic (dashed), and cross (dotted) terms, respectively. Both κ_p and κ_k remain positive while κ_{kp} is always negative [30].

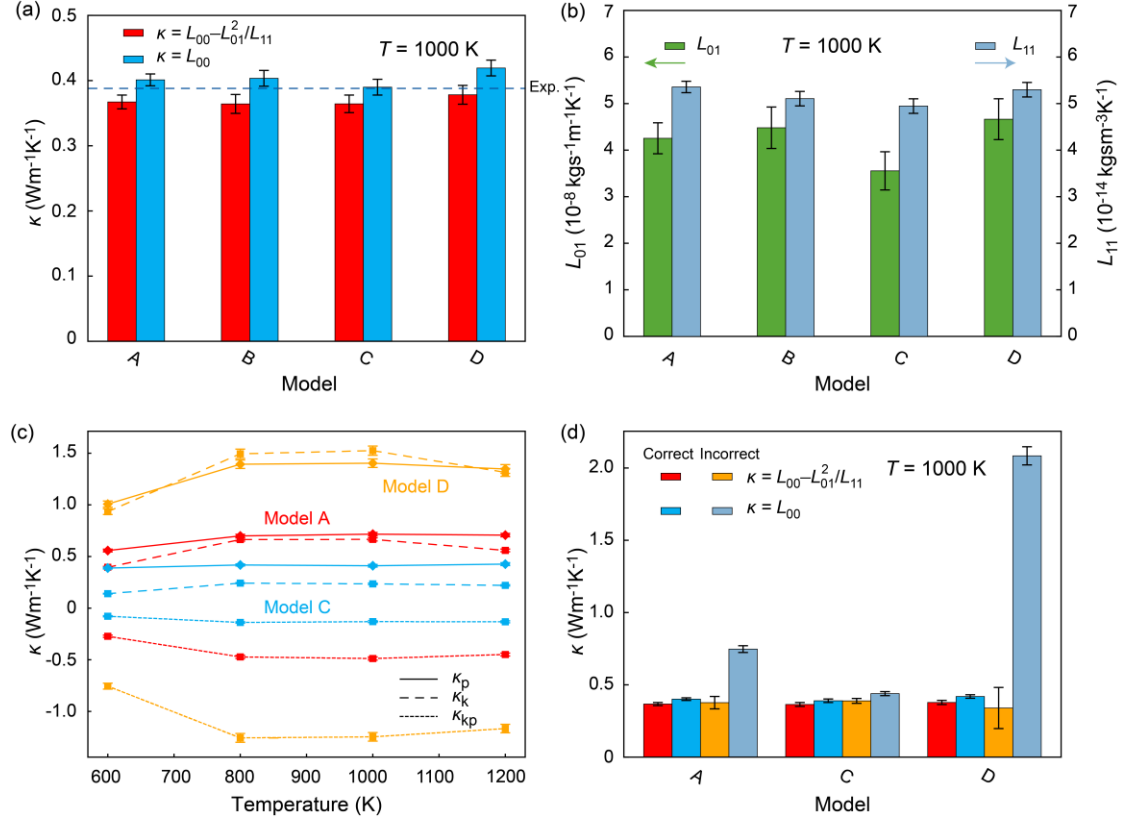


FIG. 4. Thermal conductivity and Onsager coefficients of β -Cu_{1.98}Se. (a) Thermal conductivity at 1000 K obtained from the direct Green-Kubo integral of energy flux L_{00} (blue) and the formula $L_{00} - L_{01}^2/L_{11}$ (red) using different machine-learned models. Experimentally measured thermal conductivity at 1000 K is also plotted (blue dashed line) [14], where the electronic contribution has been subtracted for direct comparison. (b) L_{01} and L_{11} of β -Cu_{1.98}Se at 1000 K. (c) Thermal conductivity L_{01} decomposition into κ_p , κ_k , and κ_{kp} based on the energy flux as a function of temperature. (d) Thermal conductivity of β -Cu_{1.98}Se at 1000 K obtained by using the correct and incorrect energy flux formula.